A NEW CAD SYSTEM FOR EARLY DIAGNOSIS OF DETECTED LUNG NODULES

Ayman El-Baz[1], Georgy Gimel'farb[2], Robert Falk[3], and Mohamed Abo El-Ghar[4]

[1]Bioengineering Department, University of Louisville, Louisville, KY, USA
[2]Department of Computer Science, University of Auckland, New Zealand.
[3] Director Medical Imaging Division, Jewish Hospital, Louisville, Kentucky, USA.
[4] Urology and Nephrology Department, University of Mansoura, Mansoura, Egypt.

ABSTRACT

A pulmonary nodule is the most common manifestation of lung cancer. Lung nodules are approximately-spherical regions of relatively high density that are visible in X-ray images of the lung. Large (generally defined as greater than 1 cm in diameter) malignant nodules can be easily detected with traditional imaging equipment and can be diagnosed by needle biopsy or bronchoscopy techniques. However, the diagnostic options for small malignant nodules are limited due to problems associated with accessing small tumors, especially if they are located deep in the tissue or away from the large airways; therefore, additional diagnostic and imaging techniques are needed. One of the most promising techniques for detecting small cancerous nodules relies on characterizing the nodule based on its growth rate. The growth rate is estimated by measuring the volumetric change of the detected lung nodules over time, so it is important to accurately measure the volume of the nodules to quantify their growth rate over time. In this paper, we introduce a novel Computer Assisted Diagnosis (CAD) system for early diagnosis of lung cancer. The proposed CAD system consists of five main steps. These steps are: i) segmentation of lung tissues from low dose computed tomography (LDCT) images, ii) detection of lung nodules from segmented lung tissues, iii) a non-rigid registration approach to align two successive LDCT scans and to correct the motion artifacts caused by breathing and patient motion, iv) segmentation of the detected lung nodules, and v) quantification of the volumetric changes. Our preliminary classification results based on the analysis of the growth rate of both benign and malignant nodules for 10 patients (6 patients diagnosed as malignant and 4 diagnosed as benign) were 100% for 95% confidence interval. The preliminary results of the proposed image analysis have yielded promising results that would supplement the use of current technologies for diagnosing lung cancer.

Index Terms— Diagnosis of lung cancer, lung nodule segmentation, detection of lung nodules.

1. INTRODUCTION

Lung cancer remains the leading cause of cancer-related death in the USA. In 2006, there were approximately 174,470 new cases of lung cancer and 162,460 cancer–related deaths [1]. An early diagnosis of cancer can improve the effectiveness of treatment and increase the patient's chance of survival [1, 2]. Specifically, reports by Martini et al. [2], and the National Cancer Institute's SEER program [3] demonstrated that patients identified with smaller T1 tumors had a significantly higher survival rate than patients with larger T1 tumors, which implies that early diagnosis of malignant tumors significantly decreases cancer patient mortality. Thus, there is an urgent need for new technology to diagnose small, malignant lung nodules early as well as large nodules located more than 4 cm away from large diameter airways since current technology, i.e. needle biopsy and bronchoscopy, fail to diagnose those cases.

New medical imaging modalities, including Low-Dose Computed Tomography (LDCT) and Positron Emission Tomography (PET) scans, allow for detecting smaller pulmonary nodules at earlier stages than conventional chest X–rays [4]. Various computational methods have been developed for monitoring the lung nodules detected in CT scans [5]. However, these methods do not take into account the effects of large deformation in the lung tissues due to breathing and the heart beating. In addition, these methods are not suitable for all types of lung nodules such as cavity and ground glass nodules and these methods require significant user interaction which makes them difficult for use by clinical practitioners.

2. PREVIOUS WORK

2.1. Segmentation of the lung tissues from LDCT images

There exist many techniques for lung segmentation in CT images. Sluimer et al. [6] presented a survey on computer analysis of the lungs in CT scans. The survey addresses registration of chest scans, segmentation of pulmonary structures, and their applications. Hu et al. [7] proposed an optimal gray level thresholding such that a threshold is selected using unique data set characteristics. All existing methods accurately segment normal lung tissues from low dose computed tomography but become unreliable when the lung density is affected by severe pathology of tissue attached to the lung walls. However, dense pathologies are present in approximately one fifth of the clinical scans, and it is vital for computer detection and quantification of abnormal areas that these pathologies are not missed in the initial segmentation [6].

2.2. Nodule registration

One of the most compelling motivations for identifying a potential malignant nodule is to assess its growth rate. To quantify the growth rate of a nodule, one must be able to measure the volume of nodules and to identify the corresponding nodules in a follow-up scan. The principal difficulty in estimating the nodule growth rate is automatic identification or registration of corresponding nodules in follow-up scans. Registration of pulmonary nodules is challenging due to their large displacement between the successive CT scans that may be caused by varying respiratory volumes and patient positioning. Due to these reasons, all the previous methods presume direct registration of nodule vs. nodule which is difficult to achieve, and all the previously reported systems rely heavily on user intervention for registration [5, 8].

2.3. Segmentation of the lung nodules

At present, segmentation of pulmonary nodules is under extensive study. Typical conventional techniques are based on fitting a Gaussian model to empirical data [9], but this approach becomes a chal-

lenge if initial measurements are corrupted with outliers and margin-truncation from neighboring structures. To meet these challenges, Okada et al. [10] (Siemens Corporation Research, Inc.) proposed an anisotropic intensity model fitting with analytical parameter estimation. Zhao et al. [11] proposed to segment 2D and 3D nodules based on thresholding the voxel intensity. Their algorithms accurately segment well-defined solid nodules with similar average intensities but become unreliable on cavity or non-solid nodules.

3. METHODS

Our goal is to develop and clinically validate a new image-analysis-based system for automatic follow up of detected nodules. This system will help in early diagnosis of malignant lung nodules, especially if they are located deep in the tissue or away from large airways. To achieve this goal, we propose the system shown in Fig. 1. The successive CT scan data sets taken at different times pass through several stages of processing (e.g., determination of the nodule location either manually by radiologist or automatically using our previous lung CAD detection system [12], lung segmentation, registration, etc.) to quantify the volumetric changes in the detected lung nodules.

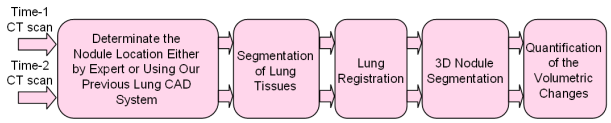

Fig. 1. Proposed system for automatic follow up of detected lung nodules for early diagnosis of malignant nodules.

3.1. Automatic detection of lung nodules

Automatic diagnosis of lung nodules for early detection of lung cancer is the goal of a number of screening studies worldwide. With the improvements in resolution and scanning time of low dose chest CT scanners, nodule detection and identification is continuously improving. We developed a new template for nodule detection using level sets which describes various physical nodules irrespective of shape, size and distribution of gray levels. The template parameters are estimated automatically from the segmented data- no a priori learning of the parameters density function is needed. We showed quantitatively that this template modeling approach drastically reduces the number of false positives in the nodule detection, thus improving the overall accuracy of CAD systems. See [12] for more detail about this approach.

3.2. Lung segmentation

Our goal is to accurately segment the lung tissues from the background in such a way that the lung borders approach closely the "ground truth" borders outlined by a radiologist. By grayness, some lung tissues such as arteries, veins, and bronchi are very close to the chest tissues. Therefore, the segmentation cannot be based only on image signals but has to account also for 3D spatial relationships between signals and region labels in order to preserve the details. The main idea of the proposed segmentation algorithm is based on accurate identification of both the spatial interaction between the lung voxels and the intensity distribution for the voxels in the lung tissues (Fig. 2). We proposed a new technique for unsupervised segmentation of multi-modal grayscale images such that each region-of-interest relates to a single dominant mode of the empirical marginal probability distribution of gray levels. We follow the most conventional description of the initial images and desired maps of regions by a joint Markov-Gibbs random field (MGRF) model of independent image signals and interdependent region labels, but we focus on more accurate model identification [13]. To better specify region borders, each empirical distribution of image signals is precisely approximated by a linear combination of Gaussians (LCG) with positive and negative components [13]. We modify the Expectation-Maximization (EM) algorithm in [13] to deal with the LCG and also exploit our novel EM-based sequential technique to get a close initial LCG-approximation to start with. The proposed technique identifies individual LCG-models in a mixed empirical distribution, including the number of positive and negative Gaussians. Then the initial LCG-based segmentation is iteratively refined using the MGRF with analytically estimated potentials [13]. The analytical estimation is the key issue that makes the proposed segmentation accurate and fast and therefore suitable for clinical applications (mathematical details of this approach are presented in [13]). Figure 3 shows the segmentation results of three LDCT data sets using the proposed segmentation approach.

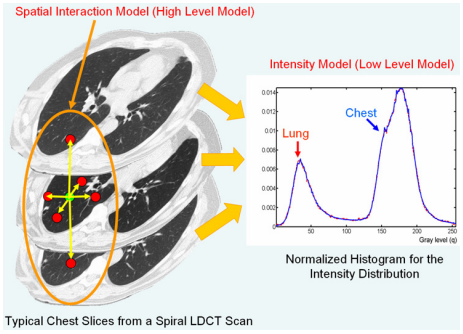

Fig. 2. Illustration of spatial interaction and intensity models.

Fig. 3. 3D segmentation results of lung tissues from LDCT images.

3.3. Lung registration

The main steps of our registration technique being essential for quantifying the volumetric changes (the growth rate) in the detected lung nodules are outlined below.

3.3.1. Global registration

In this paper, we present a novel approach to align 3D data of a textured object (lung) with a given prototype (reference data) based on learning prior visual appearance model of the reference data. In the medical imaging context, learning the visual appearance model means to model the relation between the voxels' signals (gray levels) and represent this relation in numbers, large numbers mean strong relation. In order to achieve this goal, we use Markov-Gibbs random field with pairwise interaction [13] to model the relation between the voxels in the 3D data sets after normalizing their signals. The reference and target data are normalized using the cumulative empirical probability distributions of their signals to account for monotone (order-preserving) changes of signals (e.g. due to different illumination or sensor characteristics). The similarity to the prototype (reference data) is measured by a Gibbs energy [14] of signal

co-occurrences in a characteristic subset of voxel pairs derived automatically from the prototype. An object is aligned automatically by an affine transformation that maximizes the similarity using the gradient search algorithm.

MGRF based appearance model: Given a neighborhood system $\mathcal{N}$ and potential $\mathbf{V}$, the Gibbs probability $P(g)$ is exponentially proportional to Gibbs energy $(E(g))$ of an object g aligned with the learned prototype (reference data) g° on 3D lattice $\mathbf{R}_{\mathsf{p}}$ is specified with the Gibbs energy:

$$E(g) = |\mathbf{R}_{\mathsf{p}}|\mathbf{V}\mathbf{F}^{\mathsf{T}}(g) \tag{1}$$

where $\mathbf{F}^{\mathsf{T}}(g)$ is the vector of scaled empirical probability distributions of signal co-occurrences over each clique family, $|\mathbf{R}_{\mathsf{p}}|$ is the cardinality of $\mathbf{R}_{\mathsf{p}}$, and T indicates transposition.

To identify the Gibbs energy in Eq. (1) which describes the appearance model of 3D texture prototype, we have to estimate the neighborhood $\mathcal{N}$ and the potential $\mathbf{V}$ from g°. Using the analytical approach similar to that in [14], the potentials are approximated with the scaled centered empirical probabilities:

$$\mathbf{V} = \big(\mathbf{F}(g^{\circ}) - \frac{1}{Q^2}\mathbf{U}\big);$$

where $\mathbf{U}$ is the vector with unit components and Q is the number of gray levels.

To find the characteristic neighborhood set $\mathcal{N}$, the relative energies for the clique families, i.e. the scaled variances of the corresponding empirical co-occurrence distributions, are compared for a large number of possible candidates. To automatically select the characteristic neighbors, we consider an empirical probability distribution of the energies as a mixture of a large "non-characteristic" low-energy component and a considerably smaller characteristic high-energy component: $P(E) = \pi P_{\mathrm{lo}}(E) + (1-\pi)P_{\mathrm{hi}}(E)$. Both the components $P_{\mathrm{lo}}(E)$, $P_{\mathrm{hi}}(E)$ are of arbitrary shape and thus are approximated with linear combinations of positive and negative Gaussians [13]. For more detail see [14]

Appearance-based registration: The object g is affinely transformed to maximize its relative energy $E(g_{\mathbf{a}}) = \mathbf{V}^{\mathsf{T}}\mathbf{F}(g_{\mathbf{a}})$ under the learned appearance model $[\mathcal{N}, \mathbf{V}]$. Here, $g_{\mathbf{a}}$ is the part of the object image reduced to $\mathbf{R}_{\mathsf{p}}$ by the affine transformation. Figure 4(d) shows checkerboard visualization between the data sets shown in Fig. 4(a) and the aligned data set shown in Fig. 4(c) to demonstrate the effect of the motion of the lung tissues. It can be seen that the connectivity, at the edges of the lung, between the two volumes is not smooth when using global model only, this is due to the local deformation which comes from breathing and heart beats

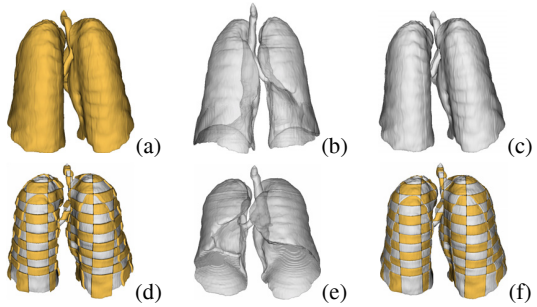

Fig. 4. (a) Reference data, (b) target data, (c) transformed data using 12 degree of freedom affine transformation, (d) checkerboard visualization to show the motion effect of the lung tissues, (e) our non-rigid regeneration results, and (g) checkerboard visualization to show the quality of the proposed local deformation model.

Local motion model: To handle local deformations, we propose a new approach based on deforming the object over evolving closed and equi-spaced surfaces (iso-surfaces) to closely match the reference data [15]. The evolution of the iso-surfaces is guided by an exponential speed function by minimizing the distances between corresponding pixel pairs on the iso-surfaces on both images [15]. The normalized cross correlation is used to find the correspondent points between these iso-surfaces [15].

The first step of our approach is to generate the distance map inside the object using fast marching level sets [16]. The second step is to use this distance map to generate iso-surfaces. Note that the number of iso-surfaces, which is not necessarily the same for both images, depends on the accuracy and the speed required by the user. The third step consists in finding the correspondences between the iso-surfaces using normalized cross correlation. The final step is the evolution of the iso-surfaces; here, our goal is to deform the iso-surfaces in the first data set (target image) to match the iso-surfaces in the second data set. Figure 4(e, f) shows the results after applying the local deformation model, it shows the connectivity, at the edges of lung region, and between the two volumes is smoother when using the proposed local deformation model.

The main advantage of the proposed local deformation model is its generality (e.g., is not limited to a certain medical image modality), computational speed, and finally its accuracy in preserving the local shape following the registration procedure.

3.4. Segmentation of lung nodules

The fourth step of the proposed framework is to accurately segment, after the data alignment, the lung nodules from the CT data. To separate each pulmonary nodule from its background in a CT chest image, we will use two new adaptive probabilistic models of visual appearance of small 2D and large 3D pulmonary nodules to control the evolution of a deformable boundary [17, 18]. The prior appearance will be modeled with a translation and rotation invariant MGRF with pairwise interaction of voxel intensities. The MGRF is analytically identified from a set of training nodules. Visual appearance of the nodules and their background at each current step of evolution will also be represented with a mixed marginal probability distribution of voxel intensities in chest images to be modeled with the LCG models. Details of these appearance models are given in [17, 18]. Figure 5 shows the segmentation results of the proposed lung nodule segmentation approach.

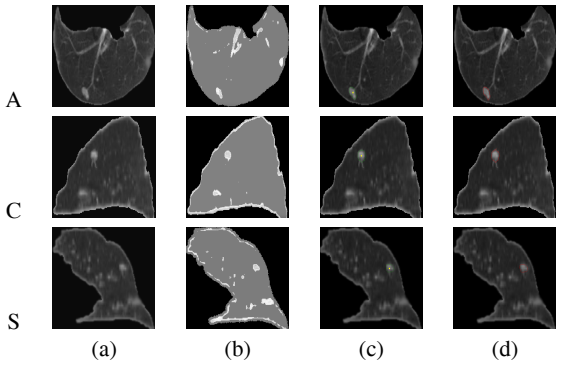

Fig. 5. 3D segmentation of pleural attached nodules; results are projected onto 2D axial (A), coronal (C), and saggital (S) planes for visualization: 2D profile of the original nodule (a), pixel-wise Gibbs energies (b), our segmentation (c), and (d) the radiologist's segmentation.

4. EXPERIMENTAL RESULTS AND CONCLUSIONS

The proposed system tested on the clinical datasets collected from the 10 patients to illustrate the significance of our methodology of measuring the growth rate. The data in this paper are collected from subjects over 60 years of age with positive smoking history (more than 10 packs/year). These subjects underwent screening with LDCT every three months for one year, so each patient has five scans with a slice thickness of 2.5 mm reconstructed every 1.5 mm, scanning pitch 1.5mm, KV 140, MA 100, and F.O.V 36 cm. These 10 patients were diagnosed by biopsy (ground truth); of them, 6 patients have malignant nodules and 4 have benign nodules.

Figure 6 shows the estimated growth rate for two detected lung nodules before and after data alignment. It is clear from Fig. 6 that our alignment algorithm facilitates accurate evaluations of changes in the nodule size over time. Moreover, the alignment would help radiologists/doctors to track the direction of nodule growth which is crucial for the treatment by surgery or radiation. Also, it is apparent that the malignant nodule doubles in size in a time period less than or equal to 360 days, while the volumetric changes in the benign nodule are very small (maximum 6% over one year, see Figure 7). Figure 7 shows volumetric changes for 6 malignant and 4 benign nodules. It is clear that the growth rate of the malignant nodules is higher than the growth rate of the benign nodules, and this encourages us to use the growth rate as a discriminatory feature between the malignant and benign nodules.

Our preliminary diagnosis results based on the analysis of the growth rate of both benign and malignant nodules for 10 patients (6 patients diagnosed as malignant and 4 diagnosed as benign) were 100% correct under the 95% confidence interval. These results show that the use of the proposed image analysis techniques could be a promising supplement to current technologies for diagnosing lung cancer. In our future work, we aim to build a probabilistic model for the growth rate of both benign and malignant nodules from 200 patients; this probabilistic model will help us to develop a complete image based software system for automatic diagnosis of lung cancer.

Patient #1				
Scanning periods	After 3 months	After 6 months	After 9 months	After 12 months
Before Alignment	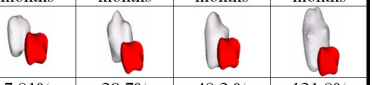			
ΔV	7.91%	28.7%	49.2 %	121.9%
After Alignment	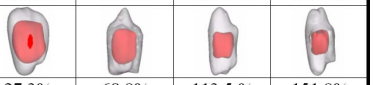			
ΔV	27.3%	68.9%	113.5 %	151.9%
Patient #2				
Scanning periods	After 3 months	After 6 months	After 9 months	After 12 months
Before Alignment				
ΔV	0.96%	1.7%	5.71%	8.9%
After Alignment	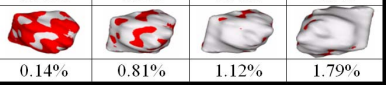			
ΔV	0.14%	0.81%	1.12%	1.79%

Fig. 6. The results of the proposed follow up registration algorithm for two patients (patients # has maligninant nodule and patient #2 has benign nodules) over one year

5. REFERENCES

[1] American Cancer Society: Cancer Facts and Figures, 2006.

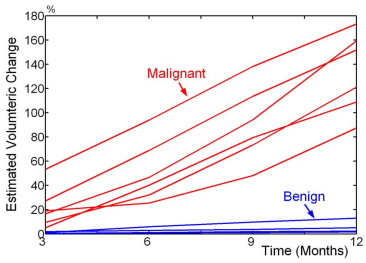

Fig. 7. Estimated percentage volumetric changes for 6-maligninat and 4-benign nodules

[2] M. Kris, et al., "Primary chemotherapy in stage IIIA no-small cell lung cancer patients with clinically apparent mediastinal lymph node metastases: focus on five-year survivors," *Lung Cancer*, vol.9, pp. 369–376, 1993.

[3] Alliance for Lung Cancer Advocacy, Support, and Education: Early Detection and Diagnostic Imaging, 2001.

[4] R. Falk, et. al., Jewish Hospital Lung Cancer Screening, Report Dated 10/20/2000, pp. 25.

[5] A. Reeves, et al., "On measuring the change in size of pulmonary nodules," *IEEE Trans. Medical Imaging*, vol. 25, no. 4, pp. 435–449, April 2006.

[6] I. Sluimer, et al., "Computer Analysis of Computed Tomography Scans of the Lung: a Survey," *IEEE Trans. on Medical Imaging*, vol. 25, no. 4, pp. 385–405, 2006.

[7] S. Hu, E. A. Hoffman, and J. Reinhardt, "Automatic Lung Segmentation for Accurate Quantitation of Volumetric X-ray CT Images," *IEEE Trans. Medical Imaging*, vol. 20, no. 6, pp. 490-498, June 2001.

[8] C. Yankelevitz, et al., "Small Pulmonary Nodules: Volumetrically Determined Growth Rates Based on CT Evaluation," *Radiology*, vol. 217, no. 1, pp. 251–256, 2000.

[9] K. Fukunaga, *Statistical Pattern Recognition,* San Diego: Academic, 1990.

[10] K. Okada, D. Comaniciu, and A. Krishnan, "Robust Anisotropic Gaussian Fitting for Volumetric Characterization of Pulmonary Nodules in Multislice CT," *IEEE Trans. Med. Imaging*, vol. 24, pp. 409–423, 2005.

[11] B. Zhao, D. Yankelevitz, A. Reeves, and C. Henschke, "Two-Dimensional Multicriterion Segmentation of Pulmonary Nodules on Helical CT Images," *IEEE Trans. Medical Imaging*, vol. 22, pp. 1259–1274, 2003.

[12] A. Farag, A. El-Baz, et al., "Quantitative Nodule Detection in Low Dose Chest CT Scans: New Template Modeling and Evaluation for CAD System Design," Proc. of MICCAI, Palm Springs, California, USA, October 26–29, 2005, pp. 720–728.

[13] A. Farag, A. El-Baz, and G. Gimel'farb, "Precise Segmentation of Multi-modal Images," *IEEE Transactions on Image Processing*, vol. 15, no. 4, pp. 952-968, April 2006.

[14] A. El-Baz, et al., "A Novel Approach for Image Alignment Using a Markov-Gibbs Appearance Model," *Proc. of International Conference on Medical Image Computing and Computer-Assisted Intervention (MICCAI'06)*, Copenhagen, Denmark, pp. 734–741, October, 2006.

[15] R. Fahmi, A. Abdel-Hakim, A. El-Baz, and A. Farag, "New Deformable Registration Technique Using Scale Space and Curve Evolution Theory and a Finite Element Based Validation Framework," *Proc. of the 28th Annual Int. Conf. of the IEEE Engineering in Medicine and Biology Society*, New York, NY, Aug–Sep, 2006, pp. 3041–3044.

[16] J. A. Sethian, "Fast marching level set method for monotonically advancing fronts," *Proc. Nat. Acad. Sci., USA*, vol. 93, pp. 1591–1595, Feb. 1996.

[17] A. Farag, A. El-Baz, et al., "Appearance Models for Robust Segmentation of Pulmonary Nodules in 3D LDCT Chest Images," *Proc. of MICCAI'06,* Copenhagen, Denmark, October 1–6, 2006, pp. 662-670.

[18] A. El-Baz, et al., "A Framework for Automatic Segmentation of Lung Nodules from Low Dose Chest CT Scans," Proc. of ICPR'06, Hong Kong, August 2024, 2006, pp. 611-614.